Removal of Pb^{2+} from contaminated water using modified multiwalled carbon nanotubes

L. S. Molele[a], T. Magadzu[a,*], A. A. Ambushe[b]
[a]*Department of Chemistry, University of Limpopo, Private Bag X 1106, Sovenga, Polokwane, 0727, South Africa*
[b]*Department of Chemical Sciences, University of Johannesburg, P.O. Box 524, Auckland Park, 2006, South Africa*

The effects of ethylene diamine (EDA), poly (amidoamine) (PAMAM) dendrimer and polyvinyl alcohols (PVA) modified multi-walled carbon nanotubes (MWCNTs) were investigated for the adsorption of Pb^{2+} ions in synthetic water and subsequently, in wastewater samples. The prepared MWCNTs nanocomposites were confirmed by Fourier transform infrared (FTIR) spectroscopy, X-ray diffraction (XRD), thermogravimetric analysis (TGA), transmission electron microscopy (TEM) and scanning electron microscopy (SEM). The concentration of Pb^{2+} ions were measured by flame-atomic absorption spectroscopy (F-AAS) and inductively coupled plasma-mass spectroscopy (ICP-MS), respectively. Removal of Pb^{2+} ions from synthetic solutions was carried out by varying parameters such as pH, initial metal ion concentration, contact time and adsorbent dosage. The maximum removal of Pb^{2+} ions was achievable at a pH of 6.5. The removal efficiency increased (more than 90%) with metal ion concentration; and reached equilibrium at 40 mg/L Pb^{2+} ions in all nanocomposites. Equilibrium was reached within the first 30 minutes, (at a low adsorbent dosage of 0.03 g) and remained constant in all nanocomposites. The EDA-MWCNTs nanocomposite yielded more than 90% Pb^{2+} ions removal from synthetic solutions as compared to both PAMAM dendrimers and polyvinyl alcohols. The analysis of wastewater indicated that the concentration of Pb^{2+} before treatment was ranging from 4.09 to 35.73 µg/L. The nanocomposite was able to remove 99% of Pb^{2+} from wastewater. Concentrations of Pb^{2+} varied from 0.200 - 0.234 µg/L after adsorption, which are below acceptable levels recommended by World Health Organisation (WHO), i.e, 10 µg/L Pb^{2+}.

(Received May 20, 2021; Accepted August 16, 2021)

Keywords: Adsorption, Multi-walled carbon nanotubes, Wastewater, Ethylenediamine, Lead (Pb^{2+})

1. Introduction

South Africa is one of the leading producers of a wide range of precious metals in the world [1]. Unwanted waste containing heavy metals are discharged into the environment and contaminate water. Heavy metals are hazardous to the environment and the communities near various industries because during heavy rains, they are washed and deposited into rivers as sediments [2, 3]. Among these heavy metals, lead ions easily accumulate in various water bodies. In water it exists as Pb^{2+}, which makes it easier to enter food chains and accumulates in body soft tissues [4]. In the past, the environment was more populated with lead emissions to ambient air due to its emission from petrol. Fortunately, in developing countries it has decreased due to introduction of unleaded petrol [5]. In wastewater, lead originates from battery manufacturing, printing, painting, dying and other industries [6]. The maximum permissible level (MPL) of lead in drinking water as stated by World Health Organisation (WHO) is 10 µg/L [7]. It can enter the body through digestive system or lungs; and if it is in large quantity this will result in cancer, anaemia, renal kidney, headache, abdominal pains and various symptoms relayed to nervous system [8, 9].

* Corresponding author: takalani.magadzu@ul.ac.za

Several techniques have been applied for removal of heavy metals and these includes reverse osmosis and nano-filtration, ion exchange, membrane separation, precipitation and adsorption [10, 11]. Amongst all methods, adsorption technology is preferred due to its low cost, high efficiency and its simplicity of operation towards the removal of heavy metals [12]. Although, several commercially available adsorbents exist such as activated carbon, inorganic oxides, and chitosan/natural zeolites, their applications are limited due to low sorption capacities and efficiencies [13].

Several researchers have proven that multi-walled carbon nanotubes (MWCNTs) are capable of removing heavy metals from water due to their unique structural properties such as large surface area, high porous hollow structure, high adsorption rate and high thermal stability [14]. For example, a study undertaken by Mubarak *et al*. [15] has shown that MWCNTs are capable of rapidly adsorbing Pb^{2+} from aqueous solution. However, their applications are limited due to formation of bundles that are held together by weak Van der Waals forces, which complicate their dispersity in various solvents. To subvert this, MWCNTs are mainly polymerised with a variety of polymers, which enhances their adsorption capacity due to improved interfacial adhesion strength. For example, studies conducted elsewhere using MWCNTs modified with ethylene diamine (EDA) [16] and poly (amidoamine) (PAMAM) dendrimers [17] showed enhancement of the dispersity and the heavy metal adsorption [18-20] of the composite materials. The type of branches and terminal functional groups attached on the core of the PAMAM can be controlled, which makes it easier to modify MWCNTs [20]. The polyvinyl alcohol (PVA_1 and PVA_2 of two different molecular weights) modified MWCNTs Zhang *et al*. [21] showed an improved strength of composite. Furthermore, the studies undertaken by Lin *et al*. [22] have shown that PVA has good chelating properties, which are envisaged to enhance the adsorption of Pb^{2+}.

Although, Zang *et al*. [18] have reported the heavy metal adsorption properties of EDA-MWCNTs composite, the focus was mainly on solid-phase extraction and pre-concentration of metal ions in synthetic batch studies. Hence, this study has investigated the effects of EDA, PAMAM dendrimer and polyvinyl alcohol (PVA_1 and PVA_2) on MWCNTs towards their dispersity and adsorption of Pb^{2+} from both synthetic and wastewater, collected from Lephalale Municipality in Limpopo Province, South Africa.

2. Materials and methods

2.1. Materials

All reagents were of analytical grade and were used as received for all experiments, unless otherwise stated. Calibration standards and sample preparation were carried out using double de-ionised water obtained from an ultra-pure water purification unit (Milli-Q® Reference, Merck) with a resistivity of 18.2 MΩ.cm at 25 °C. Anhydrous acetone and methanol were obtained by adding about 10 g of calcium or magnesium sulphate.

Multiwalled carbon nanotubes (MWCNTs, 110-170 nm x 5-9 μm, purity ≥ 99%), nitric acid (HNO_3 puriss p.a, 65%), hydrogen peroxide (H_2O_2 puriss p.a, 30%,), ethylene diamine ($C_2H_8N_2$ reagent Plus ≥ 98%), polyvinyl alcohol (PVA hydrolysed ≥ 99%), ethylene glycol ($C_2H_6O_2$ reagent Plus ≥ 99%), dimethyl sulfoxide (DMSO C_2H_6OS Bioreagent ≥ 99.7%), aluminium chloride ($AlCl_3$ 99% trace metals), N,N'-Dicyclohexylcarbodiimide (DCC, $C_{13}H_{22}N_2$ puriss ≥ 99.0%), methyl acrylate ($C_4H_6O_2$ 99%), toluene-2,4-diisocyanate ($C_9H_6N_2O_2$ 80% technical grade), acetone (C_3H_6O ACS reagent ≥ 99.5%), methanol (CH_3OH ≥ 99.9% absolute AR), and calcium sulphate ($CaSO_4$ reagent Plus, ≥ 99%), were all purchased from Sigma Aldrich.

Standards solutions were prepared daily using stock solution of lead standard (Pb^{2+} pure plus single element in 2% HNO_3), obtained from Sigma Aldrich. The solutions' pHs were adjusted using sodium hydroxide (1 M NaOH ACS Reagent ≥ 98%) and hydrochloric acid (1 M HCl ACS reagent, 37%) obtained from Sigma Aldrich. Nylon membrane filter papers (0.45 um x 47 mm) were purchased from Rochelle Chemicals & Lab Equipment Close Corporation.

For wastewater and river water sample analysis, the standard reference materials (SRMs) used for validation of the analytical methods is an SRM 1643f - Trace elements in water (NIST, USA).

2.2. Preparation of adsorbents

Prior to functionalisation with EDA, PAMAM dendrimer and polyvinyl alcohol (PVA_1 and PVA_2), MWCNTs were sonicated for 3 h at 25 ^oC using a mixture of H_2O_2 and HNO_3 (55%) in a ratio of 3:1 (v/v). Thereafter, the acid treated MWCNTs were diluted with de-ionised water and filtered through a 0.45 µm nylon membrane until a neutral pH is reached and then dried under vacuum at 80 ^oC for overnight [23]. The prepared acid treated MWCNTs were denoted as COOH-MWCNTs.

2.2.1. Synthesis of EDA-MWCNTs composite

The EDA-MWCNTs were prepared following the method described elsewhere [18], with modification. Briefly, about 2 g of COOH-MWCNTs were suspended in 75 mL of EDA under stirring at 80 °C. The mixture was allowed to reflux at 80 °C, for 48 h under nitrogen atmosphere. Then the product was filtered, washed off and then dried under vacuum at 80 ^oC.

2.2.2. Synthesis of PVA-MWCNTs composite

The PVA-MWCNTs were prepared following the method described elsewhere [24], with slight modification. Since PVA exists in many different molecular weights, the small molecular weight ranging between 13.00 g/mol and 23.00 g/mol (PVA_1) was chosen together with high molecular weight ranging between 146.00 g/mol and 186.00 g/mol (PVA_2).

Approximately 0.2 g of COOH-MWCNTs was added to a mixture of 2 g of PVA_1 and 20 mL dimethyl sulfoxide in a three-necked round bottomed flask equipped with a magnetic stirrer. The mixture in the flask was slowly heated from room temperature to 90 °C and when the PVA was completely dissolved, 1 g of $AlCl_3$ which serves as a catalyst, was added. The mixture was continually stirred at 70 °C for 24 h under a nitrogen atmosphere. The reaction was terminated by pouring the mixture into a solution of methanol mixed with hydrochloric acid (volume ratio 1:1). The product was centrifuged at 3000 rpm for 15 min and the precipitates were washed with de-ionised water several times until no apparent $AlCl_3$. Finally, the PVA_1-MWCNTs composite was obtained after drying under vacuum at 80 ˚C for 3 h. A similar procedure was followed to prepare a PVA_2-MWCNTs composite.

2.2.3. Synthesis of PAMAM-MWCNTs composite

Firstly, about 0.5 g of COOH-MWCNTs was dispersed in an anhydrous acetone (20 mL) under stirring for 30 minutes, followed by drop-wise addition of 4 mL toluene 2.4-diisocyanate. The amidation reaction by toluene 2,4-diisocyanate was undertaken in a dry nitrogen atmosphere at 25 °C for 24 h. After 24 h, the functionalized NCO-MWCNTs were washed with anhydrous acetone to completely remove the residuals, filtered and left to dry at room temperature overnight [17].

The next step involved dispersing about 0.3 g of produced NCO-MWCNTs in 20 mL of anhydrous acetone under sonication for 30 minutes, and then an excess ethylenediamine (about 10 mL) was added while stirring at 25 °C for 24 h. The resulting solid was washed with anhydrous methanol, filtered and dried overnight (80 °C) in a vacuum, generating NH_2-MWCNT [25].

The last step of formation of PAMAM on MWCNTs surface was initiated by NH_2-MWCNTs involving the Michael addition of methyl acrylate (MA) on peripheral amino groups as follows: Briefly, 0.1 g of NH_2-MWCNTs was dispersed in methanol (20 mL) while stirring and then 40 mL of methanol/MA solution (1:1) was added and the mixture was allowed to react at 30 °C for 48 h. The resulting product was filtered, washed, and dried, yielding functionalized MWCNTs containing the "first generation" ester group (MWCNTs-$G_{0.5}$-$COOCH_3$) (Pan *et al*., 2006). The amidation of the terminal groups of $COOCH_3$-MWCNTs was carried out by the same procedure as discussed above (except using EDA instead of MA). The product was washed with methanol, filtered, and dried, yielding functionalized MWCNTs containing the "first generation" amino groups (NH_2-G_1-MWNTs) [26].

2.3. Characterisations

The structure of all prepared composites was carried out by XRD with CuKα (1.5405Å) radiation. The morphology of the nanocomposites was examined by SEM (JSM 5910, JEOL 5910/Japan). For functional groups assessment FTIR (Thermo Nicolet 6700/USA) was used. TEM (JM 2100, JEOL, Japan) was used for identification of the surface structure of the nanocomposites. The TGA analyses were performed using a Perkin Elmer STA 6000 to monitor the thermal stability of the MWCNTs composites. The batch experiments were monitored using a Perkin Elmer Pinnacle 500 flame-atomic absorption spectrometry (F-AAS) (United States), equipped with an innovative touchscreen interface, which is flexible to operate through its easy-to-use Syngistix Touch software or the more comprehensive, optional **Syngistix™** for AA Software with operating conditions indicated in Table 1.

Table 1. The operating condition for F-AAS for Pb.

Operating Conditions	Pb
Measuring Wavelength (nm)	283.3
Lamp Current value (mA)	10.0
Slit Width (nm)	0.5
Burner height (mm)	7.0
Oxidant	Air
Flow of C_2H_2 (L/min)	2.0

Perkin Elmer Sciex Elan 6100 inductively coupled plasma-mass spectrometry (ICP-MS) (Germany) was employed for detection of trace elements in water samples. The instrument was equipped with quartz torch, nickel sampler and skimmer cones, a peristaltic pump, a cyclonic type pneumatic nebulizer and a double pass Scott-type spray chamber. The summary of operating conditions is indicated in Table 2.

Table 2. The ICP-MS operating conditions.

Parameter	Settings
Nebulizer gas flow	1.0 L/min
Auxiliary gas flow	1.2 L/min
Plasma gas flow	14 L/min
ICP RF power	1400 L/min
Lens voltage	10 V
Analogue stage voltage	-2550 V
Pulse stage voltage	1050 V
Torch box temperature	30 °C
Cooling system: Main temp. and interface water temp.	18.0 °C & 32.6 °C

2.4. Pb^{2+} ions adsorption experiments

Batch experiments were conducted to study the effects of solution pH value (2 - 8), contact time (2 - 60 min), initial metal ion concentration (20 - 100 mg/L) and adsorbent dosage (0.03 - 0.13 g). Typically, approximately 0.05 g of nanocomposites (as adsorbents) were added into a 100 mg/L Pb^{2+} ion solution (10 mL) in 100 mL beakers and stirred vigorously for specific time to facilitate adsorption of the Pb^{2+} ion onto the adsorbents. The pH was adjusted to the respective value using a 0.1 M HCl and 0.1 M NaOH. The adsorbents-solution mixtures were filtered through a nylon membrane of 0.45 µm, and the metal concentrations were analysed before and after adsorption using F-AAS. The effects of initial metal ion concentration were studied by

adding 0.05 g of nanocomposites into 10 mL of Pb^{2+} ions, with the concentration ranging between 20 and 100 mg/L. The removal rates (%) were calculated using equation 1.

$$R = \frac{C_i - C_f}{C_i} \times 100\% \quad (1)$$

where, C_i (mg/g) and C_f (mg/g), are the initial and final concentration of Pb^{2+} ions, respectively and R is the removal rate (percentage) of Pb^{2+} ions. The m (mg) is the mass of adsorbent, and V (mL) is the volume of solution [27].

3. Results and discussion

3.1. Characterisation of nanocomposites

3.1.1 TGA analysis of COOH-MWCNTs, EDA-MWCNTs, PAMAM-MWCNTs and PVA-MWCNTs

The data in figure 1 shows the TGA profiles of (a) COOH-MWCNTs, (b) PVA_2-MWCNTs, (c) PVA1-MWCNTs, (d) PAMAM-MWCNTs, (e) EDA-MWCNTs, (f) pure PVA_1 and (g) pure PVA_2. Prior to the TGA analysis no pre-treatment of samples was performed; hence the moisture vaporisation weight loss peak was observed in most samples starting from 50 to 110 °C. The data indicates that COOH-MWCNTs (figure 1a) is stable up to 550 ºC and an approximately 4 wt.% loss was observed from 150 ºC, which can be associated with adsorbed water and some CO_2 evolution of the carboxylic group attached to the surface of CNTs. Similar behaviour was reported by Canete-Rosale *et al*. [16].

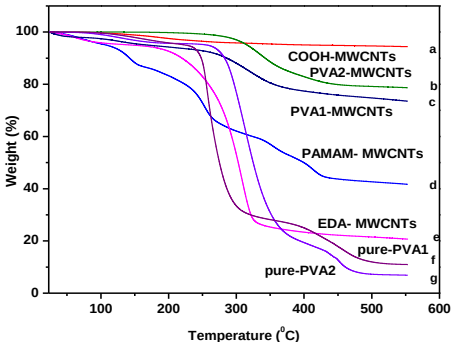

Fig. 1. The TGA profiles for (a) COOH-MWCNTs, (b) PVA_2-MWCNTs, (c) PVA_1-MWCNTs (d) PAMAM-MWCNTs, (e) EDA-MWCNTs, (f) pure PVA_1 and (g) pure PVA_2. All samples were not pretreated to remove moisture, prior to TGA analysis.

The TGA profiles of PVA-MWCNTs with different molecular masses portray related weight loss with different decomposition temperatures. Moreover, the PVA_1-MWCNTs (Figure 1c) appear to have a low decomposition temperature, as compared to PVA_2-MWCNTs (Figure 1b). This might be due to an increase in the number of chains which are strongly covalently bonded together (in the case of PVA_2-MWCNTs). The profiles of two pure PVAs with different molecular masses are also displayed in figure 1f and 1g. The thermal behaviour of the two pure samples agrees with the study by Zawawi *et al*. [28]. It was noted that pure PVA displays three distinct weight loss stages, i.e., from 30 to 210 °C (5 wt. % loss of weakly physisorbed water), 210 to 400 °C (decomposition of side chain of PVA), and 400 to 450 °C (decomposition of main chain of PVA). A sequential weight loss is detected for PAMAM-MWCNTs composite (figure 1d), which can be associated with the number of generations of PAMAM covalently bonded to the walls of MWCNTs. It has been reported that the number of generations of PAMAM dendrimer increases

the quantity of PAMAM on the walls of MWCNTs [26]; hence, a stepwise decomposition from 150 to 340 ºC is observed. The TGA profile of EDA-MWCNTs composite (figure 1e) shows an initial weight loss of up to 150 °C, which is due to absorbed moisture. However, from 200 °C a weight loss of almost 80% is observed as compared to acid functionalised MWCNTs, which is attributed to the amine functional groups added on the surface of MWCNTs.

3.1.2. The XRD patterns of COOH MWCNTs, EDA-MWCNTs, PAMAM-MWCNTs, pure PVA and PVA-MWCNTs

The data in figure 2 shows the XRD profiles of different nanocomposites used in the study. The main XRD peak profile of COOH-MWCNTs (figure 2a) strongly exhibits graphitic characteristics due to their intrinsic nature; and the indexed peaks at 26.8°, and 39.8º 2θ are due to (002) and (100) planes, respectively [29]. The attachments of EDA on the surface of MWCNTs decreased the graphitic peak intensity on EDA-MWCNTs [30], which confirms a successful addition of EDA group on the surface/walls of MWCNTs.

The PVA is a crystalline polymer in nature, hence the broad sharp diffraction peak at 2θ = 23.4º is a characteristic profile of PVA crystalline structure [31]. The intensity of a peak at 23.4º 2θ of a pure PVA (figure 2d) now appears as a hump on PVA_2-MWCNTs (figure 2e) (similar XRD features were observed on PVA_1-MWCNTs, not shown), which confirms successful modification [32]. This data supports the presence of approximately 20% of PVA on MWCNTs, as noted on TGA profiles.

The characteristic crystallinities of MWCNTs in PAMAM-MWCNTs (figure 2c) composite are not visible on XRD patterns. This could be attributed to insufficient content of MWCNTs or the encapsulation of MWCNTs by polymer (as confirmed by SEM data in figure 5d), hence the decrease in intensity of peaks. Similar features were reported by Veerapandian *et al*. [33].

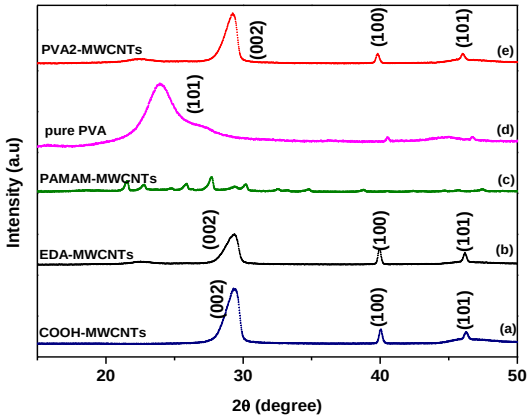

Fig. 2. XRD profiles for (a) COOH-MWCNTs, (b) EDA-MWCNTs, (c) PAMAM-MWCNTs (d) pure PVA, (e) PVA_2-MWCNTs.

3.1.3 The FTIR spectra of pristine MWCNTs, COOH-MWCNTs, EDA-MWCNTs, PAMAM-MWCNTs and PVA-MWCNTs

Oxidation of MWCNTs brought up hydroxyl and carboxylic acid groups as shown in figure 3a. The stretching band at 3220 cm^{-1} is attributed to O-H functional groups. An aromatic ring peak attributed to C=C was slightly observed at 1560 cm^{-1}. The appearance of peak at 1250 cm^{-1} is associated with C-O stretching vibrations of carboxylated anions. Similar findings were reported by several researchers [34; 35]. A smooth band at 3375 cm^{-1} is attributed to the primary amine stretching vibration of EDA-MWCNTs (figure 3b), while peak at 1750 cm^{-1} is assigned to -NH_2 bending, as reported by Rahimpour *et al*. [36]. The presence of peak at 1635 and 1250 cm^{-1} correspond to N-H bending and C-N stretching mode of aliphatic amines groups, respectively. This is in agreement with the data reported by Jimeno *et al*. [37].

The FTIR profile of PAMAM-MWCNTs (figure 3c) composites shows the presence of a sharp band at 1750 cm^{-1}, which correspond to an amide C=O stretching vibration; hence a successful modification of MWCNTs has been achieved. Furthermore, the profile shows a peak at 1659 cm^{-1} and 1500 cm^{-1}, which correspond to the amine stretching and bending mode, respectively. The characteristic peaks of C-N group are observed at 1009 cm^{-1} that shows a family of PAMAM dendrimer, as reported by Barakat *et al*. [19] and Maleki et al. [38].

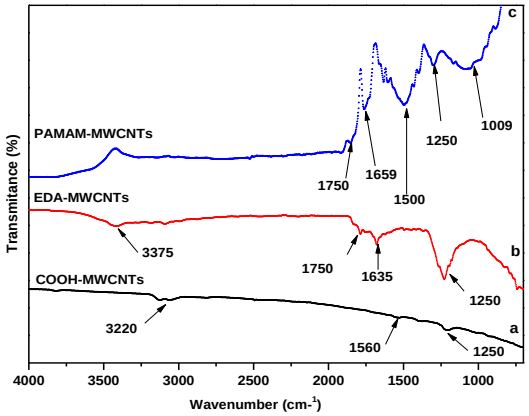

Fig. 3. FTIR spectra of (a) COOH-MWCNTs, (b) EDA-MWCNTs and (c) PAMAM-MWCNTs.

The FTIR profiles of PVA_1, PVA_2, PVA_1-MWCNTs and PVA_2-MWCNTs are as shown in figures 4. Pure PVA_1 (figure 4) have an absorption band of hydrogen bonded O-H peak above 3000 cm^{-1} [39], which is the only broad peak when the alcohol is not dissolved in a solvent. However, in the study undertaken the O-H peak is relatively sharp because MWCNTs was modified with PVA dissolved in high boiling point solvent (DMSO) and further washed with excess de-ionised water until neutral pH achieved. Since PVA is made-up of long chains, the peaks below 1000 cm^{-1} are attributed to the bending motion associated CH_2 groups in an open chain. These spectra are thoroughly explained in the book of Pavia *et al*. [40]. These long-chain bands prove that MWCNTs were successfully modified by PVA.

It has been reported that an important absorption band in all PVAs is verified at frequencies between 1100 cm^{-1} and 1000 cm^{-1}, and these vibrational band are mostly attributed to the crystallization of PVA, related to carboxyl stretching band C–O. It has been further used as an assessment tool of PVA structure and was reported by other researchers as well [41, 42].

The FTIR spectra of PVA_1- and PVA_2-MWCNTs, shows an absorption bands at 2992 cm^{-1} and 2951 cm^{-1} which is attributed to C-H stretching (Figure 4). Furthermore, peaks at 1760 cm^{-1} and 1768 cm^{-1} corresponds to the C=O stretching. Moreover, 1562 cm^{-1} and 1508 cm^{-1} presents the characteristics of bending C-H groups, superposition C-H, and deforming O-H group. The peaks above 3000 cm^{-1} corresponds to the O-H stretching vibrations of carboxylic acid in all the nanocomposites spectra. Similar results were reported elsewhere [41, 21].

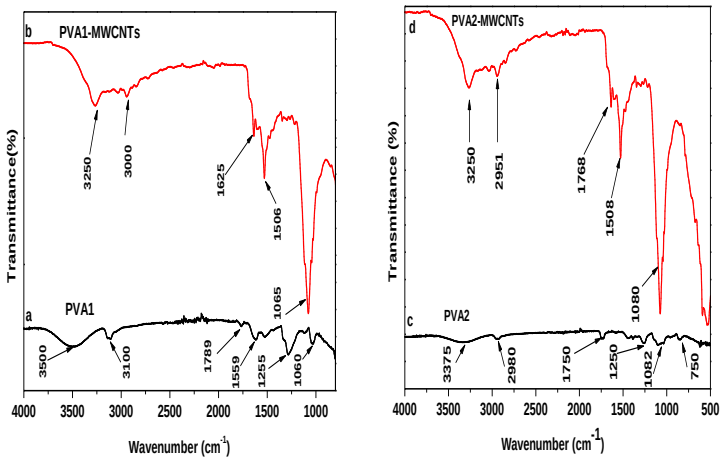

Fig. 4. FTIR spectra of (a) PVA_1 (b) PVA_1-MWCNTs, (c) PVA_2 and (d) PVA_2-MWCNTs.

3.1.4. SEM images of COOH-MWCNTs, EDA-MWCNTs, PAMAM-MWCNTs, PVA_2-MWCNTs and pure PVA

The morphology of the prepared nanocomposites was further characterised by SEM as shown in figure 5. The SEM data in figure 5 shows the images of COOH-MWCNTs (figure 5(a1)), EDA-MWCNTs (figure 5(b1)), PAMAM-MWCNTs (figure 5(c1)) and PVA_2-MWCNTs (figure 5(d1)). The surface of COOH-MWCNTs (figure 5(a1)) was cleaned during oxidation process by removing carbonaceous species such as amorphous carbon [43]. Moreover, compact stacking morphology was exhibited and no disordered debris with entangled-like structures was observed. Similar observation was made by Ma *et al*. [44]. The EDA-MWCNTs nanocomposite (figure 5(b1)) shows no agglomeration, which is attributed to the grafting of amino group on the surface of MWCNTs. Moreover, the EDA-MWCNTs nanocomposite appears to be brighter than COOH-MWCNTs (Figure 5(a1)). This might be due to exposure to EDA functional groups, which increases the MWCNTs surface reflection, as suggested by Hadavifar *et al*. [45]. The PAMAM-MWCNTs nanocomposite (figure 5(c1)) shows a dense white spongy-like image of polymeric matrix encapsulating the MWCNTs [44]. It can further be noted that MWCNTs tubes are invisible on the grid surface, which support the weakening of graphitic peak of MWCNTs as seen on XRD profile for PAMAM-MWCNTs (figure 2c).

The SEM image of MWCNTs incorporated with PVA is depicted in figure 5(d1). The pure PVA (figure 5(e1)) present a uniform morphology with smooth surface and irregular shape in comparison with PVA_2-MWCNTs (figure 5(d1)). It became gradually rough and spongy when combined with MWCNTs (figure 5(d1)), which may result in stronger interaction between MWCNTs and the polymer [46]. Moreover, the thin film of PVA polymer keep MWCNTs apart after grafting and thus disable the nanocomposites to agglomerate and entangle [46]. The two PVA with different molar masses portrayed similar characteristics upon incorporation on MWCNTs.

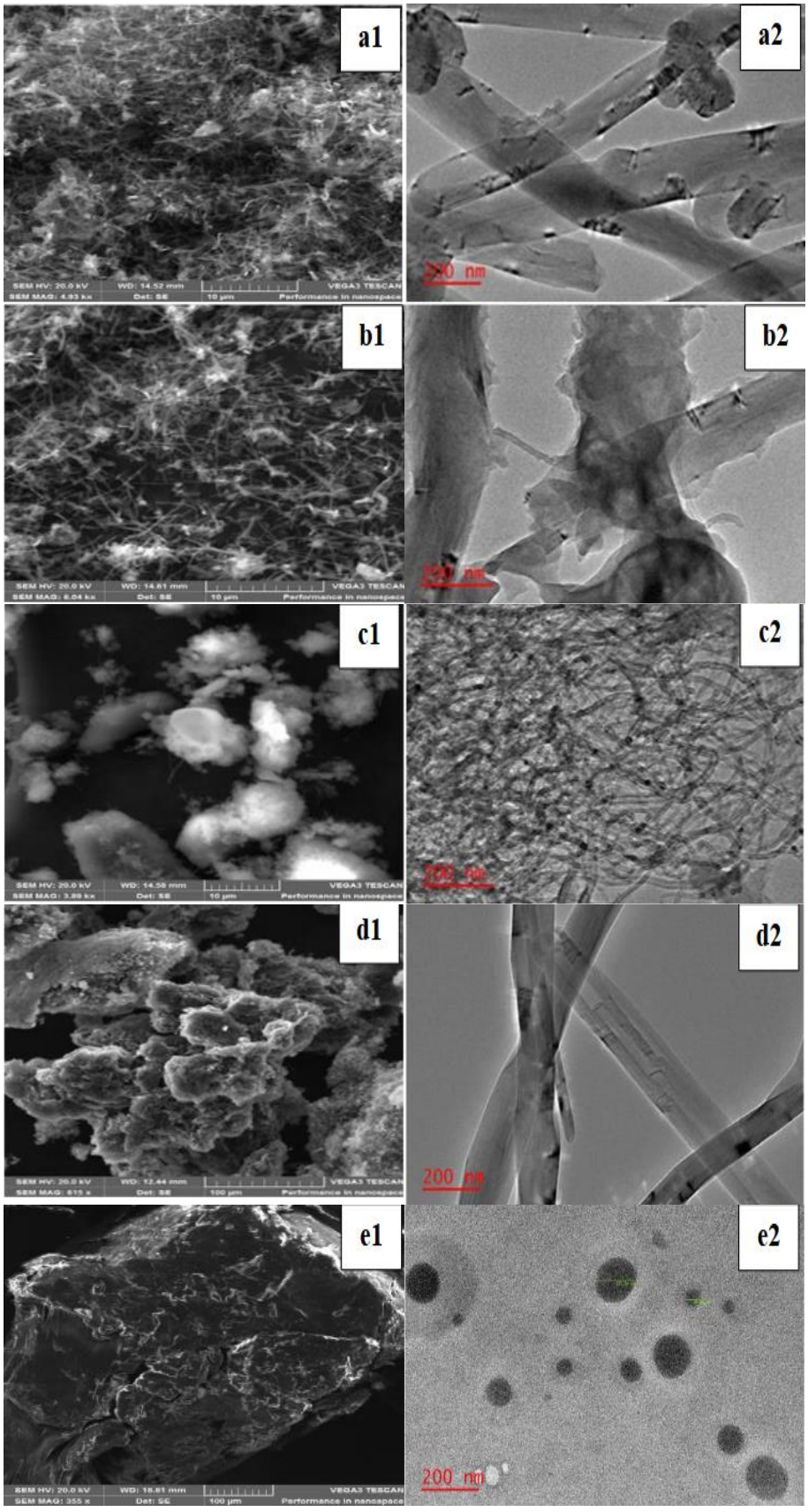

Fig. 5. SEM images of (a1) COOH-MWCNTs, (b1) EDA-MWCNTs, (c1) PAMAM-MWCNTs, (d1) PVA_2-MWCNTs and (e1) pure PVA and their corresponding HRTEM images (a2, b2, c2, d2, e2).

3.1.5. TEM images of COOH MWCNTs, EDA-MWCNTs, PAMAM-MWCNTs. PVA_2-MWCNTs and pure PVA

The TEM surface images of COOH-MWCNTs, EDA-MWCNTs, PAMAM-MWCNTs and PVA_2-MWCNTs and found in figure 5(a2) to figure 5(d2) respectively, at 200 nm magnification. The walls of MWCNTs appear to be thick and might be due the original nature of its synthesis [47]. Acid functionalised MWCNTs (figure 5(a2)) after treatment seemed to be rough with no impurities indicating that they have been removed during oxidation process. Slight damage of the MWCNTs due to some acid treatment can be observed and XRD showed that the peak intensity was not sharp, due to a loss of the crystallinity. Fortunately, MWCNTs seemed to have not lost its properties because it was able to undergo further modifications resulting in higher removal efficiencies.

The data in figure 5(b2) and 5(c2) shows that all the TEM images of both EDA-MWCNTs and PAMAM-MWCNTs are tubular regardless of different modifications. As shown in figure 5(b2), it is clearly apparent that some portions of the MWCNTs walls are coated with EDA polymer. As compared to the acid functionalised MWCNTs, the surface walls of EDA-MWCNTs looks rougher, with the tubular structure remaining intact. Furthermore, it has exhibited thin and different morphology as compared to other nanocomposites, as reported by Bushmita *et al*. [48]. The PAMAM-MWCNTs TEM images (Figure 5(c2)) shows that the PAMAM is well dispersed with dense layer on the surface of oxidised MWCNTs, suggesting a successful attachment.

The TEM images of PVA_2-MWCNTs and pure PVA are shown in figure 5(d2) and figure 5(e2), respectively. There are spherical droplets of PVA on top of the copper grid in figure 5(e2), which appears to be smooth. Park et al. [49] has also reported similar results. Modified MWCNTs have dark spots in the tubes, which can be associated with polymer incorporated on the surface of MWCNTs. Moreover, MWCNTs have retained their tubular structure of carbon nanotubes. It can be concluded that MWCNTs has been successfully modified with PVA.

3.2. Batch adsorption studies

3.2.1 Effects of pH on adsorption of Pb^{2+} by various nanocomposites

The data in figure 7 show the effects of pH on adsorption of Pb^{2+} ions by COOH-MWCNTs, EDA-MWCNTs, PVA_1-MWCNTs, PVA_2-MWCNTs and PAMAM-MWCNTs. The data indicates that COOH-MWCNTs adsorbed a smallest, consistent amount of Pb^{2+} from low to the highest pH, with the highest removal (approximately 23%) recorded at pH of 6.5. The COOH-MWCNTs has minimum sites for adsorption, hence percentage removal was below 23%. Furthermore, COOH-MWCNTs from SEM images (figure 5b) showed the presence of carbonaceous species that restrict smooth adsorption of metal ions. Upon modification of MWCNTs, all composites except for PVA_1-MWCNTs (figure 7) had lower percentage removal of Pb^{2+} at low pH. This is due to the surface protonation of the adsorbent by H^+ ions that are in competition with metal ions for available binding active sites [12]. The maximum adsorption values were obtained at pH of 6.5, for all nanocomposites (approximately 75% Pb^{2+} ions removal), except for PVA_1-MWCNTs composite. This is because metal ions interact with unprotonated groups such as amine and carbonyl groups at high pH values [50]. A related pH effects on adsorption of Pb^{2+} was noted on the work reported by Xiong *et al*. [29], though their maximum adsorption were recorded at pH 5.8. A decrease in adsorption was obtained from 8.5 in basic conditions and is attributed to an increase in OH^- concentrations, which led to formation of metal hydroxides precipitates. Related results were reported by Tehrani et al. [50]. Surprisingly, the PVA_1-MWCNTs composite showed an initial 84% removal of Pb^{2+}, which then decreases with pH until a pH of 8.5. The three nanocomposites (EDA-, PAMAM- and PVA_2-MWCNTs composites) recorded maximum adsorption of +/-75% at pH 6.5, which differs from the results reported by Wang *et al*. [51]. They have observed the maximum adsorption of 100% at a pH 4, which could be due to a very low concentration of Pb^{2+} used in the batch studies.

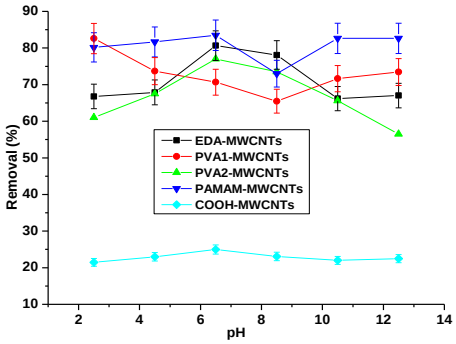

Fig. 7. Effect of pH on adsorption of 20 mg/L Pb^{2+} by nanocomposites.

3.2.2. Effects of concentrations on the adsorption of Pb^{2+} by various nanocomposites

The data in figure 8 show the effect of concentration on adsorption of Pb^{2+} by various nanocomposites at pH of 6.5. The COOH-MWCNTs had low removal of Pb^{2+}, as compared to all other nanocomposites.

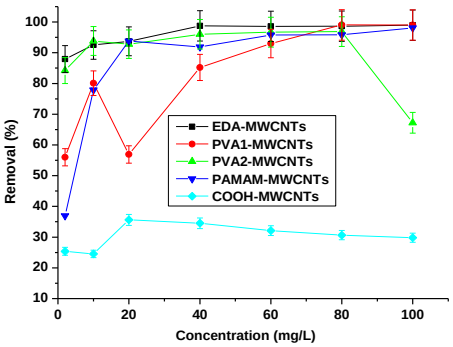

Fig. 8. Effect of initial concentration on Pb^{2+} adsorption by nanocomposites.

An increase in Pb^{2+} removal was noted, when the concentration increased from 5 - 10 mg/L Pb^{2+}, which then decreases as the concentration increases up to 100 mg/L. All four modified MWCNTs composites showed a rapid exponential growth of Pb^{2+} removal as the concentration increases, with the stability (surface saturation) being reached at approximately 20 - 60 mg/L. Similar adsorption trends where observed on various adsorbents [52, 29]. Both PVA_2- and EDA-MWCNTs showed the highest adsorption at initial concentration, with EDA-MWCNTs attaining the optimum adsorption at 40 mg/L. This suggests that the two nanocomposites have related adsorption sites at a specific adsorbent dosage.

3.2.3. Effects of contact time on the adsorption of Pb^{2+} by various nanocomposites

The data in figure 9 show the effects of contact time on adsorption of Pb^{2+}. The data indicate that within the first 30 minutes equilibrium was already reached with more than 97% removal of Pb^{2+} and these remained almost constant for 150 minutes of adsorption. Similar observation was reported by Li *et al*. [53]. The rapid uptake revealed that there was a strong adsorption affinity between Pb^{2+} and the three nanocomposites (EDA-, PAMAM- and PVA_2-MWCNTs composites) during the first 30 minutes, which is thought to be due to large number of available active sites on the adsorbents. The slight decrease might be due to the diffusion of Pb^{2+} within the pores of the nanocomposites while some adsorption taking place on some exterior surface of the adsorbents [54]. However, the MWCNTs composites surpassed the bentonite clay materials that were used by Vhahangwele *et al*. [55]. In their study for attenuation of heavy metals from acidic wastewater, the removal efficiency of less than 90% was recorded. Furthermore, the three nanocomposites also performed much better as compared to the adsorption of Pb^{2+} by

nanosilica functionalised with diethanolamine (DPM-SNPs), which adsorbed 86.10% after 60 minutes [29].

The PVA1-MWCNTs has however, showed a clear decrease from 95% to below 90% Pb^{2+} removal after 150 minutes. The COOH-MWCNTs recorded the lowest Pb^{2+} removal efficiency as compared to all nanocomposites, which emphasises the need for polymeric groups on the surface of carbon nanotubes.

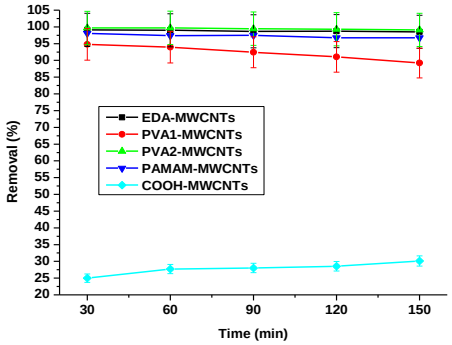

Fig. 9. Effect of contact time on Pb^{2+} adsorption by nanocomposites.

3.2.4. Effects of adsorbent dosage on the adsorption of Pb^{2+} by various nanocomposites

The data in figure 10 show the effect of adsorbent dosage on adsorption of Pb^{2+} by various nanocomposites. All nanocomposites, except COOH-MWCNTs had an initial adsorption efficiency above 85% at an initial dosage of 0.03 g. Interesting to note is that at an initial dosage of 0.03 g, EDA-MWCNTs has almost achieve 100% adsorption, which then slightly decrease with an increase of adsorbent dosage. This completely differs from the trends observed as the initial concentration of Pb^{2+} is varied (section 3.2.2), which shows Both PVA_2- and EDA-MWCNTs nanocomposites displaying related adsorption activities. At a dosage of 0.03 g an EDA-MWCNTs has shown better adsorption properties as compared to Tris(2-Aminoethyl) Amine, which recorded 95% removal of Pb^{2+} ions [50].

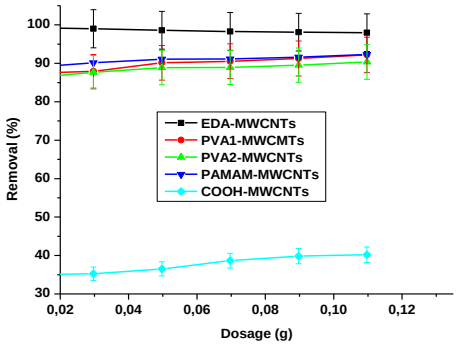

Fig. 10. Effect of adsorbent dosage on Pb^{2+} adsorption by nanocomposites.

3.3. Removal of Pb^{2+} from polluted water using EDA-MWCNTs nanocomposite

The concentrations of contaminated water samples collected from four different study areas in the Limpopo province were analysed by ICP-MS before application studies using EDA-MWCNTs nanocomposite to investigate its effectiveness as compared to the data obtained on simulated water samples during batch studies. The samples were collected from Mankweng, Polokwane, Seshego and Lebowakgomo wastewater treatment plants as well as in Mokolo River in Lephalale. The EDA-MWCNTs nanocomposite was chosen because of the highest adsorption efficiency (95%) as compared to all other nanocomposites. Furthermore, the optimum pH (6.5), contact time (60 min) and adsorbent dosage (0.03 g) were used.

Prior to analysis of samples, the method should be validated to check accuracy of the procedure undertaken throughout using standard reference material of trace elements in water. The SRM 1643f was analysed to determine the accuracy of the method employed for water sample analysis. The SRM 1643f with the certified concentration of 18.4 ± 0.084 µg/L Pb^{2+} yielded a measured concentration of 20.7 ± 0.19 µg/L Pb^{2+}, which resulted in quantitative percentage recovery of 112% and acceptable for method validation.

The investigation of Pb^{2+} levels in contaminated water from four different study areas was conducted using ICP-MS. For checking the efficacy of EDA-MWCNTs nanocomposite for removal of Pb^{2+} in real water samples, two samples with high Pb^{2+} concentrations were employed. The measured concentrations before and after removal by EDA-MWCNTs nanocomposite are presented in Table 3.

Table 3. Concentrations of Pb^{2+} in water samples before and after treatment.

Sample ID	Pb (µg/L) before	Pb (µg/L) after
MK_1	35.7 ± 0.24	0.200 ± 0.04
MK_2	4.09 ± 0.41	0.234 ± 0.05

The metal ion concentrations in this study was found to be higher in samples from Mokolo River compared to other study areas due to its proximity to variety of anthropogenic activities. The removal efficiency of Pb^{2+} was found to be 99% and concentrations after treatment (0.200 and 0.234 µg/L) were far below the maximum permissible level for drinking water established by WHO [7]. This shows high efficiency of EDA-MWCNTs nanocomposite for removal of Pb^{2+} from contaminated water.

4. Conclusions

The FTIR, TGA and XRD data confirmed the successful additions of EDA, PAMAM and PVA functional groups on the surface of MWCNTs. Both SEM and TEM images have shown that the structure of MWCNTs remained intact upon modification, which is further supported by a slight decrease of the characteristic graphitic peak of MWCNTs. The maximum adsorptions of Pb^{2+} by most nanocomposites were obtained at a pH of 6.5, which is closely related to the pH acceptable for potable water. The data indicate that the three nanocomposites (EDA-, PAMAM- and PVA_2-MWCNTs composites) have good adsorption rate for Pb^{2+} (with approximately 97% Pb^{2+} ions removal within 30 minutes). Both PVA_2- and EDA-MWCNTs showed good adsorption as the concentration increases, with EDA-MWCNTs attaining approximately 97% adsorption at an initial adsorbent dosage of 0.03 g. Hence, the prepared nanocomposites can be considered as cost-effective adsorbents for Pb^{2+}. The EDA-MWCNTs was able to remove 99% of Pb^{2+} from polluted water (concentrations vary from 0.200 to 0.234 µg/L after adsorption), and remainder was within the WHO acceptable levels.

Acknowledgements

This work is based on research supported by Water Research Commission (WRC) of South Africa Project Number K5/2515//1. Lizzy S. Molele acknowledges financial support received from Sasol Inzalo in partnership with National Research Foundation (NRF) Grant Number SFH170717254235, the Chemical Industries Education & Training Authority (CHIETA) and WRC during the MSc studies. The authors further acknowledge University of Johannesburg Research Centre for Synthesis and Catalysis and Spectrum for the facility.

References

[1] United States Geological Survey, http://minerals.usgs.gov/minerals/pubs/#mcs. (Accessed June 2017).
[2] K. Naicker, E. Cukrowska, T. S. McCarthy, Environ. Pollut. **122**, 29 (2003).
[3] G. Priyanka, R. T Byragi., R. P. V. V. Prasada, B. Ajay, C. V. Ramana, Int. J. Sci Nat. **7**, 866 (2016).
[4] A. Navas-Acien, E. Guallar, E. K. Silbergeld, S. J. Rothenberg, Environ. Health Perspect. **115**, 472 (2006).
[5] WHO, Guidelines for Drinking-Water Quality, 2nd ed. Volume 2-Health Criteria and other supporting information. (WHO, Geneva, 1996)
[6] R. L. Ramos, L. B. Jacome, J. M. Barron, L. F. Rubio, R. G. Coronado, J. Hazard. Mater. **90**, 27 (2002).
[7] Guidelines for drinking-water quality. 4th ed. WHO Chronicle, 38, 104. (2011).
[8] W. I. Mortada, M. A. Sobh, M. M. El-Defrawy, S. E. Farahat, Am. J. Nephrol. **21**, 274 (2001).
[9] F. Fu, Q. Wang, J. Environ. Manage. **92**, 407 (2011).
[10] L. Feini, G. Zhang, M. Qin, H. Zhang, Chin. J. Chem. Eng. **16**, 441 (2008)
[11] A. A. Khan, L. Paquiza, Desalination **265**, 242 (2011).
[12] W. Yang, P. Ding, L. Zhou, J. Yu, X. Chen, F. Jiao, Appl. Surf. Sci. **282**, 38 (2013).
[13] H. Sadegh, R. Shahryari Ghoshekandi, A. Masjedi, Z. Mahmoodi, M. Kazemi, Int. J. Nano. Dimens. **7**, 109 (2016)
[14] A. L. Page, A. C. Chang, G. Sposito, S. Mattigod, (John Wiley & Sons, New York, 1981), 182.
[15] N. M. Mubarak, F. Yusof, M. F. Alkhatib, Chem. Eng. J. **168**, 461 (2011)
[16] P. Cañete-Rosales, A. Álvarez-Lueje, S. Bollo, Sens. Actuators B Chem. **191**, 688 (2014)
[17] B. Pan, D. Cui, F.Gao, R. He, Nanotechnology **17**, 2483 (2006).
[18] Z. Zang, Z. Hu, Z. Li, Q. He, X. Chang, J. Hazard. **172**, 958 (2009).
[19] M. A. Barakat, M. H. Ramadan, M. A. Alghamdi, S. S. Algarny, H. L. Woodcock, J. N. Kuhn, J. Environ. Manage. **117**, 50 (2013).
[20] B. Hayati, A. Maleki, F. Najafi, H. Daraei, F. Gharibi, G. McKay, J. Mol. Liq. **224**, 1032 (2016).
[21] P. Zhang, D. Qiu, H. Chen, J. Sun, J. Wang, C. Qin, L. Dai, J. Mater. Chem. A **3**, 1442 (2015).
[22] H. Lin, Y. Watanabe, M. Kimura, K. Hanabusa, H. Shirai, Appl. Polym. Sci. **87**, 1239 (2003).
[23] N. B. Mkhondo, T. Magadzu, Dig. J. Nanomater. Biostructures **9**, 1331 (2014).
[24] P. Zhang, D. Qiu, H. Chen, J. Sun, J. Wang, C. Qin, L. Dai, J. Mater. Chem. A **3**, 1442 (2015)
[25] C. Zhao, L. Ji, H. Liu, G. Hu, S. Zhang, M. Yang, Z. Yang, J. Solid State Chem. **177**, 4394 (2004).
[26] W. Yuan, G. Jiang, J. Che, X. Qi, R. Xu, M.W. Chang, Y. Chen, S. Y. Lim, J. Dai, M. B. Chan-Park, J. Phys. Chem. C **112**, pp.18754 (2008).
[27] C. Xiong, S. Wang, W. Sun, Y. Li, Microchem. J. **146**, 270 (2019).
[28] N. A. Zawawi, Z. A. Majid, N. A. A Rashid, Colloid Polym. Sci. **295**, 1925 (2017).
[29] A. Aqel, K. M. A. El-Nour, R. A. Ammar, A. Al-Warthan, Arab. J. Chem. **5**, 1 (2012).
[30] M. M. Doroodmand, S. Sobhani, A. Ashoori, Can. J. Chem. **90**, 701 (2012).
[31] S. Krimm, C. Y. Liang, G. B. B. M. Sutherland, J. Polym. Sci. **22**, 227 (1959).
[32] A. M. Rashidi, M. Mirzaeian, S. Khodabakhshi, J. Nat. Gas Sci. Eng. **25**, 103 (2015).
[33] S. Veerapandian, S. Amudha, S. A. Suthanthiraraj, M. A. Rahman, A. S. Nasar, RSC Adv. **5**, 31404 (2015).
[34] E. Salehi, S.S. Madaeni, L. Rajabi, V. Vatanpour, A. A. Derakhshan, S. Zinadini, S. Ghorabi, H. A. Monfared, Sep. Purif. Technol. **89**, 309 (2012).
[35] Z. Cao, L. Qiu, Y. Yang, Y. Chen, X. Liu, Appl. Surf. **353**, 873 (2015).
[36] A. Rahimpour, M. Jahanshahi, S. Khalili, A. Mollahosseini, A. Zirepour, B. Rajaeian, Desalination **286**, 99 (2012).
[37] A. Jimeno, S. Goyanes, A. Eceiza, G. Kortaberria, I. Mondragon, M. A. Corcuera, J. Nanosci.

Nanotechnol. **9**, 6222 (2009).
[38] A. Maleki, B. Hayati, F. Najafi, F. Gharibi, S. W. Joo, J. Mol. Liq. **224**, 95 (2016).
[39] E. A. Kamoun, E. R. S. Kenawy, T. M. Tamer, M. A. El-Meligy, M. S. M Eldin, Arab. J. Chem. **8**, 38 (2015)
[40] D. L. Pavia, G. M. Lampman, G. S. Kriz, J. A. Vyvyan, Introduction to spectroscopy 4th ed. (Cram 101 Learning system 2012).
[41] H. Tadokoro, Bull. Chem. Soc. Jpn. **32**, 1252, 1334 (1959).
[42] B. J. Reddy, R. L. Frost, W. N. Martens, D. L. Wain, J. T. Kloprogge, Vib. Spectrosc. **44**, 42 (2007).
[43] Y. Sun, S. Yang, G. Sheng, Z. Guo, X. Wang, J. Environ. Radioact. **105**, 40 (2012).
[44] X. D. Ma, X. F. Qian, J. Yin, Z. K. Zhu, J. Mater. Chem. **12**, 663 (2002).
[45] M. Hadavifar, N. Bahramifar, H. Younesi, Q. Li, Chem. Eng. J. **237**, 217 (2014).
[46] I. A Safo, F. Liu, K. Xie, W. Xia, Mater. Chem. Phys. **214**, 472 (2018).
[47] B. Ruelle, S. Peeterbroeck, R. Gouttebaron, T. Godfroid, F. Monteverde, J. P. Dauchot, M. Alexandre, M. Hecq, P. Dubois, J. Mater. Chem. **17**, 157 (2007).
[48] K. Bushimata, S. I. Ogino, K. Hirano, T. Yabune, K. Sato, T. Itoh, K. Motomiya, K. Yokoyama, D. Mabuchi, H. Nishizaka, G. Yamamoto, J. Phys. Chem. C **118**, 14948 (2014).
[49] J. H. Park, S. M. Park, I. J. Kwon, J. M. Hyun, Y. Deng, Y. G. Jeong, I. W. Cheong, J. H. Yeum, J. Compos. Mater. **47**, 3367 (2013).
[50] M. S. Tehrani, P. A. Azar, P. E. Namin, S. M. Dehaghi, J. Environ. Prot. Ecol. **4**, 529 (2013).
[51] W. Wang, Chemosphere **190**, 97 (2018).
[52] S. A. Kosa, G. Al-Zhrani, M. A. Salam, Chem. Eng. J. **181**, 159 (2012).
[53] X. Li, Y. Li, Z. Ye, Chem. Eng. J. **178**, 60 (2011).
[54] K. K Wong, C. K. Lee, K. S. Low, M. J. Haron, Chemosphere **50**, 23 (2003).
[55] M. Vhahangwele, G. W. Mugera, J. Environ. Chem. Eng. **3**, 2416 (2015).